Empirical Evaluation of a Novel Lane Marking Type for Camera and LiDAR Lane Detection

Sven Eckelmann[1], Toralf Trautmann[2], Xinyu Zhang[1] and Oliver Michler[1]
[1]*Institute of Traffic Telematics, Technical University Dresden, Dresden, Germany*
[2]*Mechatronics Department, University of Applied Science Dresden, Dresden, Germany*

Keywords: LiDAR, Point Clouds, Retro Reflecting, Lane Marking, 3M, Camera.

Abstract: Highly automated driving requires a zero-error interpretation of the current vehicle environment utilizing state of the art environmental perception based on camera and Light Detection And Ranging (LiDAR) sensors. An essential element of this perception is the detection of lane markings, e.g. for lane departure warnings. In this work, we empirically evaluate a novel kind of lane marking, which enhances the contrast (artificial light-dark boundary) for cameras and 3D retro reflective elements guarantee a better reflection for light beams from a LiDAR. Thus intensity of point data from LiDAR is regarded directly as a feature for lane segmentation. In addition, the 3D lane information from a 2D camera is estimated using the intrinsic and extrinsic camera parameters and the lane width. In the frame of this paper, we present the comparison between the detection based on camera and LiDAR as well as the comparison between conventional and the new lane marking in order to improve the reliability of lane detection for different sensors. As a result, we are able to demonstrate that the track can be detected safely with the LiDAR and the new lane marking.

1 INTRODUCTION

Highly automated driving requires a zero-error interpretation of the current environment. Camera, radar, ultrasound and LiDAR sensors are primarily utilized for environmental perception and the detection of objects. In order to increase the reliability of said sensors, competing and cooperative fusion approaches can be applied. At the same time, the determination of the current position based on Global Navigation Satellite System (GNSS) sensors in combination with vehicle data, such as velocity, rotational speed of wheel and yaw rates is indispensable.

A precise information about the course of the lane is an essential prerequisite for driver assistance systems and autonomous driving and can further be used to support global positioning. Besides the comfortable lateral guidance, it serves as a reference point for further driving maneuvers such as lane change assistance or the calculation of alternative trajectories. Lane detection based on camera information has already been sufficiently handled and represents the current state of the art. Next to these conventional image processing algorithms, new approaches of machine learning are adopted. However, the basis for these types of evaluation strategies is the 2D camera, so that the 3D information are estimated by the intrinsic and extrinsic camera parameters as well as the known lane width. This estimation is accompanied by numerous false detection. Examples are glare, bitumen joints or other elements that create a similar contrast in the image (Koch et al., 2015).

1.1 Related Works

1.1.1 LiDAR Lane Detection

In literature, several approaches have been proposed using LiDAR as an input for lane detection. In (Kammel and Pitzer, 2008) the disadvantage of low resolution is compensated by increased subsequent scans, registered and accumulated employing GNSS and Inertial Measurement Unit (IMU) information. The authors in (Hata and Wolf, 2014) used a modified Otsu thresholding method and were able to detect lanes and any kind of road painting. In (Kodagoda et al., 2006) a sensor fusion algorithm to fuse images from camera and scanning laser radar (LADAR) is used to identify curbs. For this task, the solution presented in this paper used nonlinear Markov switching. The authors in (Kumar et al., 2013) extracted the lane lines by developing an algorithm that combines

Eckelmann, S., Trautmann, T., Zhang, X. and Michler, O.
Empirical Evaluation of a Novel Lane Marking Type for Camera and LiDAR Lane Detection.
DOI: 10.5220/0010550500690077
In *Proceedings of the 18th International Conference on Informatics in Control, Automation and Robotics (ICINCO 2021)*, pages 69-77
ISBN: 978-989-758-522-7

both Gradient Vector Flow (GVF) and Balloon Parametric Active Contour models. This technique was not very accurate to detect lanes at the edges of the road and the lane predicted interfered with the road curbs. The same author published a lane detection algorithm (Kumar et al., 2014) based on an intensity threshold as well as Region Of Interest (ROI) to limit the number of processed LiDAR data. Subsequently, the data was converted to a 2D image, with a linear dilation to complete rubbed off lanes. The algorithm was tested over 93 roads and managed to detect the markings in 80 roads. The authors claimed that the failures in detecting all the test roads was due to road wipings and erosion, causing small intensities and low densities to be received by the LiDAR. In (Guan et al., 2014) the point cloud is segmented into horizontal blocks. These blocks are then used to detect the edges (road curbs) based on differences in elevation in order to determine the surface as well as the road boundaries. The authors claim to accomplish a success of 0.83 of correctness to detect lane markings. In (Thuy and León, 2010) the authors developed a lane marking detection algorithm based on a dynamic threshold. First, the data points received from the LiDAR is processed using Probability Density Function (pdf), and the maximum reflectively is matched with the highest values of the pdf. The dynamic threshold is applied to this reflectively data, since the lane markings are the ones that return high reflectively (due to their color gradient). The author of (Yan et al., 2016) transformed the segmented points into scan lines based on scanner angle. Consequently, the road data is determined based on a "Height Difference" (HD). The road limits have been identified with a moving least square, that only accepts certain points that lie in a certain threshold set by the authors. Besides a classification on intensity values, the authors proposed using an "Edge Detection and Edge Constraints" (EDEC) technique that detects fluctuations in the intensity. This method should minimize the noise in the detected lanes. The algorithm was tested on data from Jincheng highway China, the authors claim that they have accomplished an accuracy level of 0.9.

1.1.2 Camera Lane Detection

Camera based lane marking detection research is a main research field and currently heavily studied. Therefore in this section, only a brief overview of related works is provided. The lane detection algorithm in (Mu and Ma, 2014) converts the raw images to grey scale and applies a Otsu's method for thresholding the image. Sobel is used to detect the lane markings. The results shows that it is effective for incomplete lane markings and for fluctuations in the environment's illumination. (Li et al., 2014) uses Canny edge detection technique which results in a binary image. Then Hough transform is implemented in order to detect the straight lines from the image. In contrast, the author of (Haque et al., 2019) uses thresholding based on gradients and the HLS color space. Followed by the perspective transformation they apply a sliding window algorithms. The centroids of the windows a finally composed to a lane.

1.2 Our Approach

For the approach presented in this paper, we tackle the main problem where lane detection in urban areas often fails, since the curving of the lane runs out of the scope from the camera. In addition most of the algorithms are mostly designed for straight lanes and not for sharp curves. Thus a reliable lane information, one of the basics for autonomous driving, is not guaranteed. In this paper we use a new type of lane marking which was developed by 3M (3M, 2021). This lane marking enhances the contrast (artificial light-dark boundary) for camera systems and the reflecting of light beam from a LiDAR with 3D arranged retro reflective elements. The intensities of the point data can directly be used as a feature for the segmentation. Complex filters are not required to extract the information from the lane marking and misinterpretations are minimized. With transferring the LiDAR points into the 2D area, the lanes are then extracted through dynamic horizontal and vertical sliding windows, which finally leads to the relevant points. For a better comparison we take the raw points into account and will not apply any filters for a smooth representation. It will also provide a comparison between the detection based on camera and LiDAR. All the measurements are done on the test field of the University of Applied Science (HTW) Dresden. Since only one lane is equipped with this new lane marker, a comparison to the conventional lane marking can be given.

2 FUNDAMENTALS

2.1 LiDAR

A LiDAR emits infrared coherent light from a laser to its environment. The energy is decisive for the classification of the sensor into the protective classes and results from the integral of the pulse over time. Due to the optics of the LiDAR, the light beam diverges and spreads flat, depending on the distance. This means that less light power is radiated onto the object in a

further distance. In addition particles in the atmosphere, like dust, fog and rain cause diffuse reflections and absorb energy from the ray. Furthermore, the surface of the object influences the reflected energy. Physical properties like total and diffuse reflection along with the kind of color have a significant impingement. In contrast to the source of the LiDAR, the light beam is reflected from the object with a full solid angle and is significantly attenuated by the scattering of infrared light. After all, the sensitivity and surface size of the receiver influence the result of the detection (Wagner et al., 2003).
The transmittance of the LiDAR is the quotient between the transmitted and the received light output. This value is colloquially known as intensity. In order to minimize the influence of attenuation by the atmosphere, the transmission power can be increased or the beam can be bundled more stronger. Another approach is to change the composition of the object color. Therefore BASF Coatings announced a new technology called cool colors or cool coatings (Coatings, 2016). This technology replaces a high proportion of ash in the paint and can reflect energy better. In addition to the cooler interior in the vehicle, LiDAR beams are also better reflected. The distance d to an object is calculated by the speed of light c and half of the appertaining run time t:

$$d = c_o \cdot t/2 \qquad (1)$$

In summery, the LiDAR is the sensor with the highest accuracy, but with increasing distance and the resulting minimization of the object-relevant back scatter pulse, the reliability and integrity of object detection reduces. At the same time, object properties such as surface texture, defined in color and gloss, relative orientation and atmospheric properties affect the back scatter intensity of the LiDAR.

2.2 Lane Markings

The examined novel type of lane marker tapes (3M, 2021) (Figure 1) have retro reflective characteristics, which are achieved by embedding glass beads. Incident light in this direction is scattered directly back. The black stripe increases the contrast to the white lane marking and therefore provides a defined contrast. This is particularly helpful on light surfaces, such as concrete. With the tall design, better visibility in rain and snow should be achieved. Originally, they were developed to improve recognition by human drivers or a camera.

The visibility in daylight as well as the retro reflective properties are defined by the Luminance Coefficient Q_d or R_L 2, which is the quotient of Luminance Density L_V [cd/m²] and Illumiance E_V [lx].

Figure 1: *Left:* Standard Lane Marking *Right:* Retro reflective lane marking tape of 3M (3M, 2021) with embedded glass beads.

$$R_L = \frac{L_V}{E_V} \qquad [\frac{\text{mcd}}{\text{m}^2\text{lx}}] \qquad (2)$$

R_L is defined in EN 1436, 2007 which defines minimum Luminance Coefficents in different classes depending on the color of the road marking, the kind of surface (alphalt or concrete) and the dampness. In addition to the new markings on the outer lane, the conventional markings are applied to the center lane and the inner lane on the test field. The retro reflective marking has a seven times higher Luminance Coefficient of $R_{L_{3M}} = 352$ comparing to the conventional lane marking of $R_{L_{conv}} = 50$.

3 EXPERIMENTAL SETUP

3.1 Vehicle

For the investigations a BMW i3 is used as test vehicle. Additional information like vehicle speed, steering angle and wheel speed are directly provided from the car via a CAN interface. All information are captured by a mini PC over Ethernet and uniquely time stamped. Thus it is possible to play back the data at a later time and to optimize the implemented algorithm.

3.2 LiDAR

For the approach, the LiDAR system Ouster OS1 is used. With a range of 120 m, a 360 ° horizontal field of view and a given angular resolution of 0.1° as well as a +/- 22.5 ° vertical field of view divided into 64 levels, it generates up to 1.310.720 points per second with a sampling frequency of 20Hz (Ouster, 2014). The LiDAR is mounted at a height of 1.8 m. Figure 2 shows the point data from the LiDAR of a measurement.

The LiDAR as well as a GNSS receiver is mounted on a mobile platform, which can easily be adapted to the roof of different vehicles.

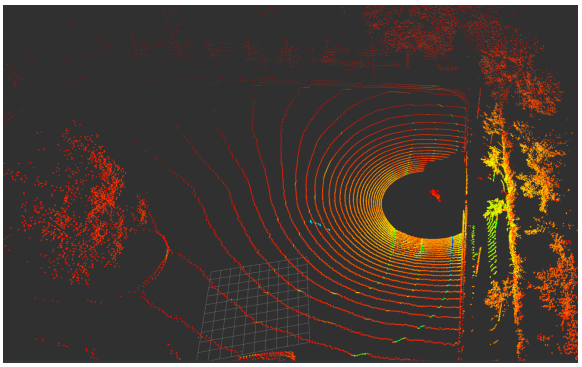

Figure 2: Recorded point cloud of a straight street on the reference track with a LiDAR sensor. The outer line is equipped with the retro reflecting lane from 3M.

3.3 Camera

In addition, a camera-based lane marking detection is evaluated. The camera used in this work is a grey scale camera (Axis M3114-R) with a resolution of 640x480 pixels. It is mounted in the center of windshield, close to the roof. A sample of the camera's raw image is shown in figure 3.

Figure 3: Rectified gray scale image frame of AXIS M3114-R (640x480).

3.4 Reference Positioning System

In order to provide a geo-reference as well as a quantitative comparison between the examined lane detection methods, the current position of the vehicle must be determined as precisely as possible. For this, an u-blox multi-constellation GNSS receiver (ublox, 2017) is utilized to estimate the current global position. They include already integrated fusion algorithm to countervail the current GNSS error. In our case we use the *automotive* and *static* setting to encourage a low deviation and thus a reliable position.

In addition we combine the output from the GNSS modules with information provided by the vehicle CAN bus system, which are the current vehicular velocity v and the yaw rate ψ. The absolute position x,y and the heading of the vehicle Θ are calculated by an Extended Kalman Filter (EKF). The state vector x_{ctrv} of the fusion model is described in 3. For the applied prediction motion model we use a Constant Turn Rate and Velocity (CTRV) model (equation 4) described in (Obst et al., 2015).

$$x_{ctrv} = (x, y, \Theta, v, \psi) \tag{3}$$

$$x_{k+1} = x_k + \begin{pmatrix} \frac{v}{\psi} * (\sin(\Theta + \psi * T) - \sin(\Theta)) \\ \frac{v}{\psi} * (-\cos(\Theta + \psi * T) + \cos(\Theta)) \\ \Theta * \psi * T \\ 0 \\ 0 \end{pmatrix} \tag{4}$$

3.5 Test Field with Reference Track

The equipped and examined track (figure 4) is part of the test field from the University of Applied Science located in Dresden, Germany. It has a dimension of approximately 50 m by 70 m. Contrary to common available data, like Open Street Map (OSM), the test field is geodetically surveyed with an high accuracy. In addition we are able to map lanes, intersections and we are able to set geographical referenced markers. The red coordinate system depicted in figure 4 represents the origin point of the local map. The surveyed data acquisition includes a complete lap around the outer test track. In addition to the LiDAR data, the data set also contains the relative position in relation to our coordinate origin (red) and raw camera data.

4 DATA PROCESSING

4.1 Camera Lane Detection

The whole workflow is given in figure 5. After rectifying the raw image in the first step, we set the ROI from the lower edge of the windshield up to the horizon, which is approximately the half of the image. In this ROI we improved the contrast and minimized the influence of ambient lighting by taking the histogram of this region in account.

A Canny edge detector followed by an morphological operation for closing unfilled regions converts the gray image to a binary. Finally we crop the image again by setting vertices of a trapezoid to reduce the influence of obstacles in the edge area. Up next,

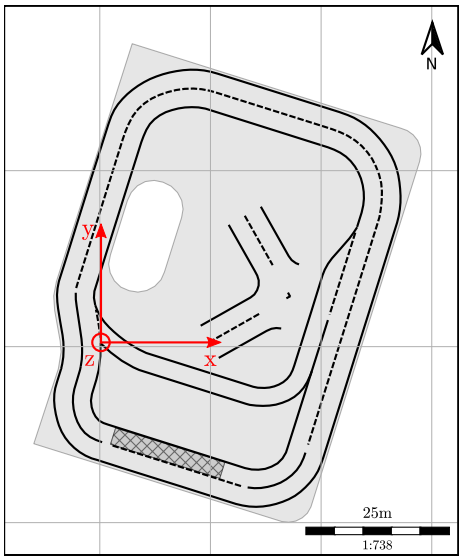

Figure 4: Reference track on the test field. The red frame represents the local coordinate system. The retro reflecting lane marking is only applied to the outer lane.

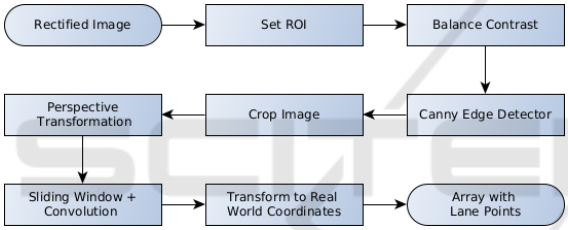

Figure 5: Workflow of the camera lane detection.

we perform a perspective transformation, which results in a bird eye view image (figure 6, *Center*). This image is the starting point for the lane detection algorithm. Therefore, we are using a sliding window starting from the lower left corner and moving horizontal to the end of the image. In each window we are using convolution to detect the maximum of white pixels. By passing a threshold, the position of the maximum convolution becomes a valid point of the lane, which we name centroid. Once we find a centroid we start going vertical in the image. Simultaneously we use the orientation of the centroid to define the next vertical window position. This vertical iteration ends, once we find no valid point and then start over from the last horizontal position. The algorithm ends once we reached the right side of the image. As result we get the relevant points of the lanes in the bird's eye perspective. Finally we can augment our centroids into the rectified image (figure 6, *Right*).

Figure 6: Examples of the camera lane detection. *Left:* Original rectified image. *Center*: Binary image in bird eye's view. The yellow points represents the segmented points and the blue points (centroids) are extracted by the sliding window algorithm. *Right:* The segmentation (yellow) and the centroids (blue) are augmented in the rectified image.

4.2 LiDAR Lane Detection

The entire workflow for LiDAR lane detection is given in Figure 7.

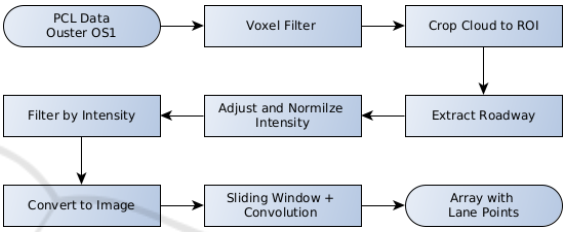

Figure 7: Workflow of the LiDAR lane detection.

We process the raw point cloud data from the LiDAR and start down sampling with a Voxel Filter and a leaf size of 0.2. We crop the point cloud to predefined ROI and focus on the relevant area in front of the vehicle. A Random Sample Consensus (RANSAC) is used to extract the roadway (cf. figure 8, *left image*). Since the intensity value decreases over the distance, we normalize and adjust that value with a linear function. Finally we set a threshold, extract the remaining lane points and convert these to an image. At this point we can use the same approach to extract the lanes with a sliding window as described in section 4.1. Finally we convert the lane points back from the image plane to the vehicle coordinate system and create optional a second degree polynomial (cf. figure 8, *right image*).

5 RESULTS

Out of the approximated lane points and our current known position (cf. section 3.4), we can transform each point of our detection algorithm into the global coordinate system, which is exemplary depicted in figure 9.

Since our test field and all lanes are geodetically surveyed we are able to compare the results with the ground truth. For evaluation and comparison, the

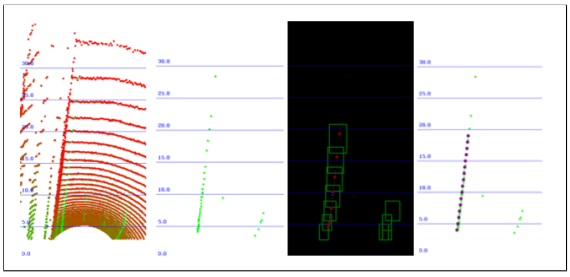

Figure 8: Examples for LiDAR Lane Detection. *Form Left to Right:* Extracted roadway as top view image; Segmented Lane with adjusted Intensity threshold; Extracting relevant lane points with sliding window algorithm; Fitted points (purple) with second degree polynomial.

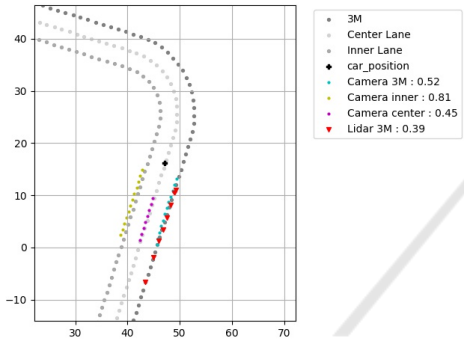

Figure 9: Transformed lanes into the global coordinate system. The ground truth is represented by the 3M -, Center- and Inner Lane and the black cross marks the current car position. The colored points represent the centroids of the detected lanes. The values of the Camera and Lidar detected lanes specify the Root Mean Square Error (RMSE) from the ground truth.

maximum length of the lane l_{Lane} , the deviation from the ground truth RMSE and the fail rate f_f (cf. equation 5) are assessed. The length l_{Lane} is defined as the distance from the center point of the car up to the farthest detected point. For calculating f_f we define that all lanes which have an higher deviation than RMSE_{max} count as not detected n_false. Since we have the same sample rate of our LiDAR and camera, we also count the number of frames where no lane was detected n_{not}. Based on the evaluation of the test drive, $RMSE_{max}$ is set to 1.5 m.

$$RMSE_{Lane} = \sqrt{\frac{1}{n}\Sigma_{i=1}^{n}\left(\frac{d_i - f_i}{\sigma_i}\right)^2} \tag{5}$$

$$f_f = \frac{n_{not} + n_{false}}{n_{frames}} \tag{6}$$

$$n_{false} = \sum_{n=0}^{Frames}(RMSE_{Lane_n} > RMSE_{max}) \tag{7}$$

5.1 Camera Lane Detection

The 3M marking can be used to examine if the contrast strip allows a better detection compared to conventional lane markings. Figure 11 shows the deviation from the ground truth for each lane and allows us to make the following statements:

- **Camera Fails in Curves:** Especially in narrow curves the lanes are running out of the cameras field of view. A detection of an inner lane marking is very unlikely. Only center and outer lane markings could be detected. Due to the structure of our text field, there is a crash barrier near the outer lane, which leads additionally to an incorrect detection.
- **Incorrectly Assigned Lanes:** The assignment of each lane to the ground truth is done by calculating the RMSE of each point to the ground truth. In that case, the course of the lane approaches the other reference track (cf. figure 10). As a result, the lanes were assigned incorrectly (cf. figure 11 at *A*).
- **Low Deviation on Straight Lanes:** In regions of straight lanes the RMSE is lower than 1.0m.
- **Uncertainty Due to Position Determination:** In *B* of figure 11 the car did not move along the center line. Additionally the uncertainty of the position determination caused a higher RMSE and a false detection.

The error rate of the 3M marking is between the middle and inner lane. At this point we cannot assess whether the 3M marking improves the lane detection, since the inner lane runs out of the field of view while passing curves and the crash barriers often causes a false detection. Furthermore, the roadway on the test field is already very dark, so that only a minimal improvement in the contrast can be achieved.

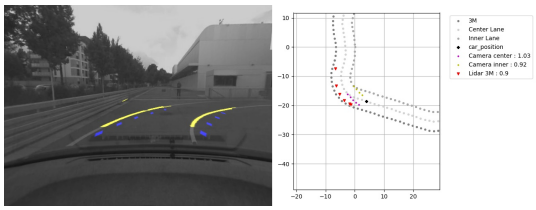

Figure 10: Error due transforming the points from the camera coordinate system into the global coordinate system.

5.2 LiDAR Lane Detection

As already mentioned, the LiDAR lane detection only takes the retro reflecting lane markings into account.

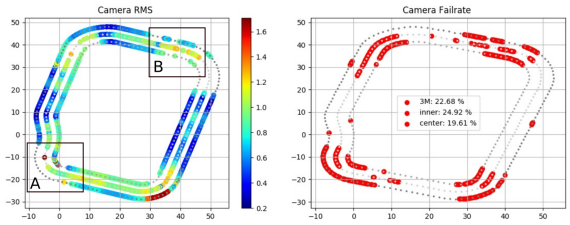

Figure 11: *Left:* RMSE from each lane to the ground truth. None colored regions are areas there the algorithm didn't detect any valid lane points n_{false}.*Right:* Represents the fail rate of the camera detection on each lane.

Thus, only the outer lane can be evaluated. Based on figure (12) we can point out the following statements:

- **Low Fail Rate:** The false detection is equally distributed on the whole track. In region *A* of figure 12 the detection fails because the segmentation returns a high intensity due to retro reflecting objects. The overall fail rate is $f_{f_{Lidar}} = 7.94\%$
- **Correctly Assigned Lanes:** The extracted lane points were assigned to the outer lane in each frame.
- **Low Deviation:** The deviation along the whole track is below 1 m. It only raises at regions where the segmentation process failed due of high intensity obstacles.

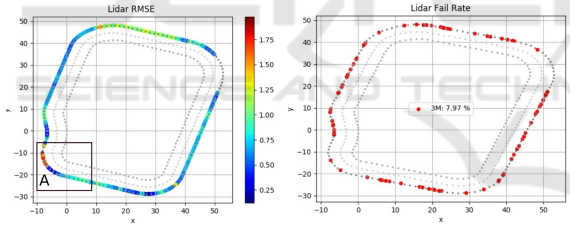

Figure 12: Lidar Lane Detection - *Left:* RMSE of the 3M lane to the ground truth. None colored regions are areas where the algorithm was not able to detect any valid lane points n_{false}. *Right:* Fail rate of the LiDAR lane detection on each lane.

5.3 Comparison of LiDAR and Camera

Figure 13 shows the length of the detected lanes. The maximum of the LiDAR and thus the prediction horizon is $l_{Lane_{Lidar}} = 30$m, compared to the camera with $l_{Lane_{Camera}} = 16$m. The lower installation position of the camera, creates a higher perspective distortion. Therefore, the area of the image, which represents the roadway and the lanes is smaller. That leads to the fact, that only few points in a smaller area can be used for subsequent processing. In addition the transformation from birds-eye-view to real coordinates fails in narrow curves, which leads to a wrong assignment of the lane (figure 10). Currently, only the camera is

Table 1: Final results of the comparison between the LiDAR and camera lane detection.

	LiDAR	**Camera**
Max Length of Lane [m]	31	16
Fail Rate of Conventional Lane Marking [%]	–	22,26
Fail Rate of 3M Lane Marking [%]	7.9	22,68
Average RMSE of Conventional Lane Marking [m]	–	0.86
Average RMSE of 3M Lane Marking [m]	0.76	0.88

able to detect multiple lanes. If we define the error rate in such a way, that at least one marking has to be recognized, the fail rate drops to 1%. The LiDAR is mounted on the roof of the car and already provides 3D data. So any perspective transformation steps do not need to be performed. The resolution of the LiDAR based on the design of the LiDAR system. In relation to our LiDAR, the vertical field of view is divided into 64 layers. The blind areas between the layers increases with the distance. As result, fewer points in the lane are recorded and changes in between can not be perceived. That also leads to the fact the the maximum length, and thus the prediction horizon depends on the visibility of each specific layer. Compared to this, the camera has a fixed and usually a higher resolution. In subject to the condition that the whole marking is visible, changes in the course of the trajectory can be better recognized.

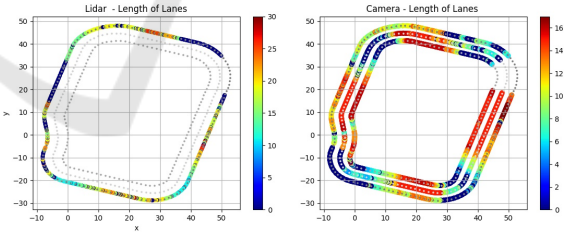

Figure 13: Length of Lane Detection - *Left:* Lidar *Right:* Camera.

Concluding, table 1 provides a comprehensive overview of all quantitative results.

6 CONCLUSION AND FUTURE WORKS

In this paper we compared a new type of lane marking (3M, 2021) using a LiDAR(Ouster OS1 (Ouster, 2014)) sensor with a camera-based lane detection. With varieties in data processing steps and coordinate

transformations, the same lane detection algorithm is applied for both sensors. The paper shows that the new lane marking together with the LiDAR gives the best results. The length of the predicted lane is two times higher and the fail rate is less than one third of the camera. It also shows, due the cameras limited field of view, narrow curves can not be detected as well. The new lane marking did not improve the detection algorithm of the camera at all. This is basically due to the already dark pavement of the test field. For future work, we will invest more research in the following topics.

- **Various Undergrounds:** Evaluating the influence of the contrast stripe on brighter roadways like concrete.
- **Various Weather Condition:** Since the new lane marking has certain height, questions like how rain and snow influences the detection should be evaluated.
- **Night Vision**: It needs to be evaluated if the retro reflecting influences the night visibility for the camera detection.
- **Combine with V2X Technology:** A Road Side Unit (RSU) could provide the information, if a lane is equipped with this special feature. Under the condition a vehicle is equipped with a LiDAR, the detection of the lane could be supported and serve as a prerequisite for highly automated driving.
- **Sensor Fusion:** A sensor fusion of camera and LiDAR would increase the reliability of the lane detection

Since 2020 where is new version of the 3M lane marking on the market. We are looking forward to equipped also the inner lane, which enables us to compare the three variants.

Besides lane marking, pole feature has seen a tremendous interest amongst research community in recent years because of their ubiquity on the urban street and stability under different weather and light conditions. It appears normally as part of street light, traffic lights and trees. In a future work we will present a new pole detection method, combining high retro reflective foils and LiDAR, which enables the calculation of lateral and longitudinal relative position of the vehicle. The test field is already equipped with nine traffic lights, which provides an excellent basis for this investigation.

Figure 14 shows the flow chart for the localization process based on pole feature. It is divided in a Pole Extractor and Particle Filter. After filtering, down sampling and segmentation, the point cloud data is extracted into multiple independent clusters. A predefined condition selects the relevant pole cluster and with the transformation it into a 2D plane, it serves as input for the localization process. Therefore we are using a particle filter. The initial position and ground truth are provided from GNSS sensor. The prediction step uses the speed and yaw rate information which are gathered from IMU. With the combination a the lane detection algorithm and the pole extraction algorithm we combine two position determination approaches, with the goal to enhance the autonomous driving.

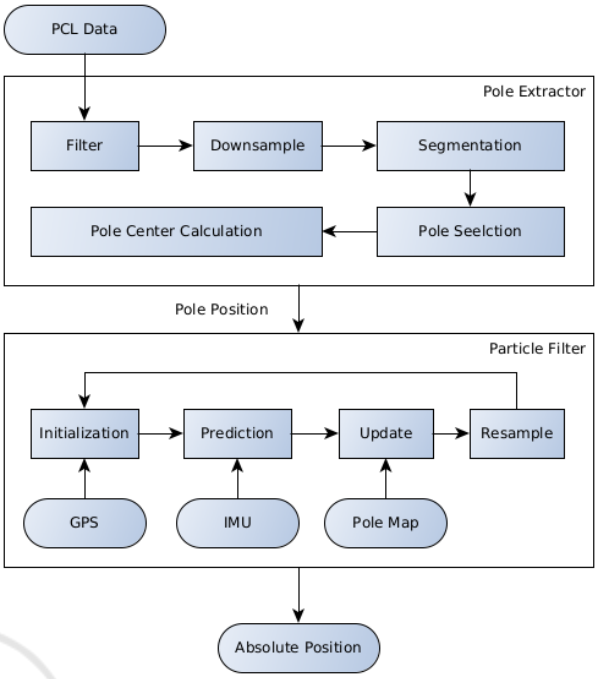

Figure 14: Flow chart for relative pose estimation with LiDAR and poles.

REFERENCES

3M (2021). 3m^{TM} stamark^{TM} high performance contrast tape 380aw-5. https://www.3m.com/3M/en_US/company-us/all-3m-products/~/3M-Stamark-High-Performance-Contrast-Tape-380AW-5/?N=5002385+8709322+3294235158&rt=rud. Accessed: 20121-02-24.

Coatings, B. (2016). Basf cool coatings. https://www.basf.com/global/de/who-we-are/organization/locations/europe/german-sites/Muenster/News-Releases/BASF-erhaelt-Bundespreis-Ecodesign-fuer-Cool-Coatings.html. Accessed: 2021-02-24.

Guan, H., Li, J., Yu, Y., Wang, C., Chapman, M., and Yang, B. (2014). Using mobile laser scanning data for auto-

mated extraction of road markings. *ISPRS Journal of Photogrammetry and Remote Sensing*, 87:93–107.

Haque, R., Islam, M., Alam, K. S., Iqbal, H., and Shaik, E. (2019). A computer vision based lane detection approach. *International Journal of Image, Graphics & Signal Processing*, 11(3).

Hata, A. and Wolf, D. (2014). Road marking detection using lidar reflective intensity data and its application to vehicle localization. In *17th International IEEE Conference on Intelligent Transportation Systems (ITSC)*, pages 584–589. IEEE.

Kammel, S. and Pitzer, B. (2008). Lidar-based lane marker detection and mapping. In *2008 IEEE Intelligent Vehicles Symposium*, pages 1137–1142. IEEE.

Koch, C., Georgieva, K., Kasireddy, V., Akinci, B., and Fieguth, P. (2015). A review on computer vision based defect detection and condition assessment of concrete and asphalt civil infrastructure. *Advanced Engineering Informatics*, 29(2):196–210.

Kodagoda, K., Wijesoma, W. S., and Balasuriya, A. P. (2006). Cute: Curb tracking and estimation. *IEEE Transactions on Control Systems Technology*, 14(5):951–957.

Kumar, P., McElhinney, C. P., Lewis, P., and McCarthy, T. (2013). An automated algorithm for extracting road edges from terrestrial mobile lidar data. *ISPRS Journal of Photogrammetry and Remote Sensing*, 85:44–55.

Kumar, P., McElhinney, C. P., Lewis, P., and McCarthy, T. (2014). Automated road markings extraction from mobile laser scanning data. *International Journal of Applied Earth Observation and Geoinformation*, 32:125–137.

Li, Y., Iqbal, A., and Gans, N. R. (2014). Multiple lane boundary detection using a combination of low-level image features. pages 1682–1687.

Mu, C. and Ma, X. (2014). Lane detection based on object segmentation and piecewise fitting. *TELKOMNIKA Indones. J. Electr. Eng. TELKOMNIKA*, 12(5):3491–3500.

Obst, M., Hobert, L., and Reisdorf, P. (2015). Multi-sensor data fusion for checking plausibility of V2V communications by vision-based multiple-object tracking. *IEEE Vehicular Networking Conference, VNC*, 2015-Janua(January):143–150.

Ouster (2014). Ouster os1 datasheet. https://data.ouster.io/downloads/OS1-lidar-sensor-datasheet.pdf. Accessed: 2021-02-24.

Thuy, M. and León, F. (2010). Lane detection and tracking based on lidar data. *Metrology and Measurement Systems*, 17(3):311–321.

ublox (2017). *NEO-M8P u-blox M8 High Precision GNSS Modules Data Sheet*. Document Number UBX-15016656, Revision R05, January 2017.

Wagner, W., Ullrich, A., and Briese, C. (2003). Der laserstrahl und seine interaktion mit der erdoberfläche. *Österreichische Zeitschrift für Vermessung & Geoinformation, VGI*, 4(2003):223–235.

Yan, L., Liu, H., Tan, J., Li, Z., Xie, H., and Chen, C. (2016). Scan line based road marking extraction from mobile lidar point clouds. *Sensors*, 16(6):903.